Transcription's bubble under the influence of long-range interactions and helicoidal coupling

Mirabeau Saha[a)†] and Timoléon C. Kofané[a)b)‡]

[a)] *Laboratory of Mechanics, Department of Physics, Faculty of Science, University of Yaoundé, P. O. Box* 812, *Yaoundé, Cameroon*
[b)] *The Abdus Salam International Center for Theoretical Physics, P. O. Box* 586, *Strada Costiera* 11, *I*-34014 *Trieste, Italy*

(Received 24 March 2013; revised manuscript received 15 June 2013)

The influence of power-low long-range interactions (LRI) and helicoidal coupling (HC) on the properties of localized solitons in a DNA molecule when a ribonucleic acid polymerase (RNAP) binds to it at the physiological temperature is analytically and numerically investigated in this paper. We have made an analogy with the Heisenberg model Hamiltonian of an anisotropic spin ladder with ferromagnetic legs and anti-ferromagnetic rung coupling. When we limit ourselves to the second-order terms in the Taylor expansion, the DNA dynamics is found to be governed by a completely integrable nonlinear Schrödinger (NLS) equation. In this case, results show that increasing the value of HC force or LRI parameter enhances the bubble height and reduces the number of base pairs which form the bubble. For the fourth-order terms in a Taylor expansion, results are closely resembling those of second-order terms, and are confirmed by numerical investigation. These results match with some experimental data and thus provide a better representation of the base pairs opening in DNA which is essential for the transcription process.

Keywords: DNA, helicoidal coupling, RNA-polymerase, spin model, Riemann zeta function, power-law long-range interaction, breather-like soliton

PACS: 94.05.Fg, 87.10.Tf, 87.14.gk, 87.53.Ay **DOI:** 10.1088/1674-1056/22/12/129402

1. Introduction

Going back to early works on solitons in biological systems[1,2] it is an old conjecture that nonlinear excitations such as kink solitons or breathers could play a functional role in the DNA dynamics, in particular in the processes of DNA denaturation and transcription. These fundamental biological processes start by the binding of a protein molecule in the specific region of the DNA molecule. A number of theoretical models through soliton-like excitations of bases, based on longitudinal and transverse motions, as well as bending, stretching, and rotation have been proposed to describe their dynamics.[3–24] For instance, Vasumathi and Daniel[25] considered protein-DNA interaction dynamics at the biological temperature, to study the base pair opening in the DNA molecule by treating it as equivalent to a spin ladder or coupled ferromagnetic lattice. This general spin-like model of DNA molecules leans on the work by Dandoloff and Saxena[26] and those by Takeno and Homma.[27,28] The efficiency of this model to describe open states in the DNA molecule was shown in these studies. In the above work by Vasumathi and Daniel,[25] the soliton excitations of the DNA bases in the two strands make localized base flipping and travel along the DNA chain in the form of a bubble. They suggested that the results may represent the bubble generated during the transcription process, when a protein such as RNAP binds to a promoter site in the DNA macromolecule.

In that study, the authors did not take into account two outstanding facts existing in the DNA molecule. The first one is the helical structure of double-stranded DNA which reinforces its geometrical structure. Indeed, a real DNA molecule has a helical shape with twisting strands and the twisting leads to the study of torsional dynamics. This double helix has 11 as helicoidal pitch. In this structure, the water filaments connect unit bases at different sites. Then, the n-th base of a strand interacts with its nearest neighbors along the physical axial direction, i.e., with the $(n+h)$-th and $(n-h)$-th bases of the complementary strand.[7,29] Referring to the earlier studies, h can take two values: 4[30,31] or 5.[32,33] The second fact is the long-range coupling between intra-strand bases which has an irrefutable impact on the DNA's dynamics. Indeed, many authors, such as Woafo *et al.*[34] and Tchawoua *et al.*[35] showed the importance to take into account the LRI in nonlinear systems. Due to the presence of phosphate groups along the DNA's strands, the LRI exists in that macromolecule and allows taking into account the screening of the interactions or an indirect coupling between base pairs through water filaments. The studies have already shown the LRI's efficiency on the DNA dynamics.[36] For instance, Rau and Parsegian[37] studied experimentally the evidence for long-range attractive hydrogen forces and emphasized that many forces could be responsible for LRI in the DNA. Larsen *et al.*[38] modeled the DNA molecule like a parabola embedded chain with LRI between a twisted base pair to study the mechanism for bubble generation.

†Corresponding author. E-mail: sahamirabeau@yahoo.fr
‡E-mail: tckofane@yahoo.com

© 2013 Chinese Physical Society and IOP Publishing Ltd

Therefore, it has become important and necessary to investigate the internal dynamics of DNA in terms of soliton bubbles by proposing a generalized model involving helicity of the molecule and LRI between intra-strand bases, i.e., nucleotides. With this in mind, in the present paper, we study the nonlinear dynamics of the DNA double helix with power law LRI between nucleotides in the same strand by proposing a generalized model for DNA dynamics along the lines of Vasumathi and Daniel's work.[25]

The remainder of the paper is outlined as follows. In Section 2, to write the model Hamiltonian, we consider the DNA molecule as consisting of two helical, interacting, molecular chains in similarity with the Heisenberg model for a coupled anisotropic site-dependent spin system. This Hamiltonian takes into account the power law LRI between intra-strand nucleotides, inter-strand hydrogen bonding, the helicoidal structure of the DNA molecule, the interaction between RNAP and DNA molecules, and the interaction between the DNA molecule and the thermal phonon. After bosonizing this Hamiltonian in the semi-classical treatment by using the Holstein–Primakoff representation of spin operators, we derive the dynamical equations and express them in the terms of coherent amplitudes of the bosonic operators. In the continuum limit, we first consider in Section 3 the lower order of the Taylor expansion and the DNA strand dynamics is governed by the NLS equation, the coefficients of which depend, among others, on LRI and HC parameters. By investigating the linear dispersion relation, the group velocity and the condition for the existence of solitonic waves are obtained. The analysis of the solitonic-like wave solution shows that the HC is weak compared to intra-strand coupling in the real DNA molecule and that increasing LRI or HC parameter increases the amplitude of the localized wave, while reducing the number of base pairs which contribute to the bubble formation. We have studied in Section 4 the dynamics of the system for the fourth order of the Taylor expansion. All in all, results show that bubble characteristics are affected by this expansion, but the influences of LRI and HC are not changed. To solve the problem of Taylor's order expansion, we carry out in Section 5 the numerical simulations which confirm analytical results. Finally, we give some concluding remarks in Section 6.

2. The model

The model under consideration is the B-form of DNA, a tertiary structure of this molecule as presented in Fig. 1(a). This form consists of two parallel chains of nucleotides known as strands with linkage internals of dipole–dipole interaction along the strands, and the strands are coupled to each other through hydrogen bonds between the complementary bases. The region where the RNAP molecule can bind, i.e., a specific segment or promoter site in the DNA molecule, is represented in this figure by a shaded ellipse overlapping the DNA double helical structure. R and R' represent the two complementary strands in the DNA double helix, and each arrow in the figure represents the direction of the bases attached to the strand. The dots between arrows represent the net hydrogen bonding effect between the complementary bases. The z axis is chosen along the helical axis of the DNA. A horizontal projection of the n-th base pair in the xy-plane is presented in Fig. 1(b). The quantities Q_n and Q'_n denote the tips of the n-th bases, and P_n and P'_n represent the points where the n-th bases are attached to the strands R and R', respectively. Figure 1(c) is a horizontal projection of the n-th base pair of the DNA in the xz-plane. Referring to Figs. 1(b) and 1(c), Homma and Takeno[17] showed that the inter-strand base–base interaction or hydrogen bonding energy between the complementary bases depends on the distance between them and using the simple geometry, they expressed the square of the distance between the tips of these bases as

$$\begin{aligned}\left(Q_nQ'_n\right)^2 &= 2+D^2+\left(z_n-z'_n\right)^2+2\left(z_n-z'_n\right)\\ &\times\left(\cos\theta_n-\cos\theta'_n\right)\\ &-2D\left[\sin\theta_n\cos\phi_n+\sin\theta'_n\cos\phi'_n\right]\\ &+2[\sin\theta_n\sin\theta'_n\left(\cos\phi_n\cos\phi'_n+\sin\phi_n\sin\phi'_n\right)\\ &-\cos\theta_n\cos\theta'_n],\end{aligned}\tag{1}$$

where D is the diameter of the circle depicted in Fig. 1(b).

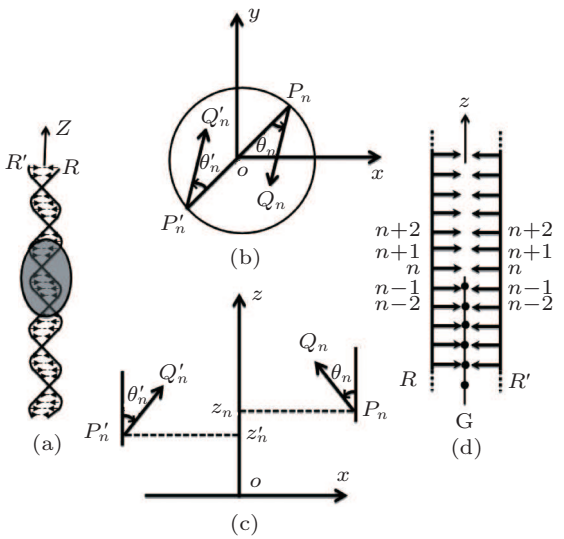


Fig. 1. (a) A schematic representation of the region where the RNAP molecule can bind to a specific segment of B-form DNA double helix. (b) Horizontal projection of the n-th base pair in the xy-plane. (c) Horizontal projection of the n-th base pair of the DNA in the xz-plane. (d) A schematic representation of the RNAP molecule binding on DNA.

This distance can be written by using quasi-spin operators as

$$\begin{aligned}\left(Q_nQ'_n\right)^2 &= 2+D^2+2\left(S^x_nS'^x_n+S^y_nS'^y_n-S^z_nS'^z_n\right)\\ &-2D(S^x_n+S'^x_n),\end{aligned}\tag{2}$$

where S_n and S'_n represent the quasi-spin operators at the lattice site n in the two legs R and R', respectively. These operators are expressed as follows:

$$S_n \equiv (S_n^x, S_n^y, S_n^z) \text{ with } S_n^x = \sin\theta_n \cos\phi_n,$$
$$S_n^y = \sin\theta_n \sin\phi_n,\ S_n^z = \cos\theta_n, \tag{3}$$
$$S'_n \equiv \left(S_n'^x, S_n'^y, S_n'^z\right) \text{ with } S_n'^x = \sin\theta'_n \cos\phi'_n,$$
$$S_n'^y = \sin\theta'_n \sin\phi'_n,\ S_n'^z = \cos\theta'_n. \tag{4}$$

Now, using the above considerations, we try to construct the Hamiltonian of our model. The Heisenberg model of the Hamiltonian for a two-coupled spin chain model or spin ladder system for DNA, which takes into account the inverse power-law type ferromagnetic LRIs between spins in the same lattice (intra-strand interaction) is written as

$$H_{\text{DNA1}} = -\sum_n \left[\sum_{m>n} \Omega_{m,n} \left(S_n \cdot S_m + S'_n \cdot S'_m\right)\right] \tag{5}$$

with

$$\Omega_{m,n} = \frac{\Omega}{|m-n|^r}. \tag{6}$$

In the summation, the term $m = n$ is excluded. The parameters r ($r \geq 2$) and Ω measure the dimensionless LRI parameter and the elastic constant of the strand, respectively. The quantity $|m-n|$ measures the absolute distance between bases n and m. The specific physical meaning of the LRI parameter depends on the following situation: $r \to \infty$ characterizes nearest neighbor interaction approximation, $r = 5$ characterizes dipole–dipole interaction between bases, and $r = 3$ characterizes Coulomb interaction between bases.[39] With the above choice, this is obviously

$$\sum_{m\neq n} \Omega_{m,n} = 2\Omega\zeta(r), \tag{7}$$

where $\zeta(r)$ represents Riemann sum, defined by

$$\zeta(r) = \sum_{n=1}^{\infty} \frac{1}{n^r}. \tag{8}$$

The two strands are coupled by the hydrogen bond interactions type. The hydrogen bond is represented by ferromagnetic or antiferromagnetic rung-coupling (inter-strand interaction). The appropriate potential is

$$H_{\text{DNA2}} = -\sum_n \beta \left(S_n \cdot S'_n\right), \tag{9}$$

where the parameter β corresponds to the inter-strand interaction constant or hydrogen bond energy constant between the complementary nucleotides. The DNA double helical chain is mapped onto a two-coupled spin chain model or a spin ladder system with $\Omega > 0$ (ferromagnetic legs) and $\beta > 0$ (ferromagnetic rungs) or $\beta < 0$ (antiferromagnetic rungs). In equilibrium state, $\beta < 0$.

To complete the description of the molecule, additional details, such as the harmonic HC due to trans-groove hydrogen-bonded water filament, should be introduced in the model. This HC models the forces between nucleotides in the complementary strands along macromolecule axis (i.e., z axis) as mentioned in the previous section. These forces maintain the helicoidal structure of the molecule. The discrete form of the free energy corresponding to the twist deformation in a cholesteric liquid crystal system is usually used to incorporate helicity in a helimagnet. Following the same line by Daniel and Beula[40] we write the Heisenberg model of the Hamiltonian corresponding to the force for the twist, which is responsible for HC in terms of spin vectors as follows:

$$H_{\text{DNA3}} = -g(S'_n S_{n+h} + S_n S'_{n+h}), \tag{10}$$

where g represents the HC coefficient. Only the nucleotides being on opposite helices at half-pitch distance are considered since they are near enough in three-dimensional space due to the double helical geometry of the DNA molecule. As the pitch of the helix corresponds to 10 or 11 bases in the B-DNA equilibrium configuration, we set $h = 5$.[32,33,41,42]

The thermal phonons due to the biological temperature of the system can affect the DNA dynamics. Thus, we generalize the above model into a thermal DNA and add the following Hamiltonian

$$H_{\text{DNA-Phonon}} = \sum_n \left[\frac{p_n^2}{2m_{\text{H}}} + \boldsymbol{K}_{\text{H}} (x_{n+1} - x_n)^2 + \alpha_1 (x_{n+1} - x_{n-1}) \left(S_n \cdot S'_n\right)\right]. \tag{11}$$

The coordinate x_n is the displacement of the hydrogen atom attached to the base at the n-th site along the direction of the hydrogen bond. Indeed, the DNA molecule works at the biological temperature, and the hydrogen atoms attached to the nucleotides are in a thermally excited state at this temperature. The parameter m_{H} is the mass of the hydrogen atom attached to the base, and K_{H} represents the elastic constant between the hydrogen atom attached to the base at the n-th site and the one attached at the $(n+1)$-th site. The quantity $p_n = m_{\text{H}}\dot{x}_n$ is the corresponding momentum and the overdot represents the time derivative. The parameter α_1 is the coupling coefficient between the rotation of bases and the vibration of the hydrogen atom attached to the base at the n-th site along the direction of the hydrogen bond in the thermal fluctuation.

We adopt a situation where an RNAP is bound to DNA. Due to the large size of this RNAP macromolecule, we consider the active site region, i.e., a small portion of the RNAP molecule which binds to the DNA molecule and initiates conformational change, as a linear chain.[43] To introduce the RNAP-DNA interaction in the Hamiltonian, the DNA promoter site is treated as a set of two coupled linear chains, in interaction with the active site region of the RNAP molecule

(see Fig. 1(d) in which the RNAP molecule is represented by G). The RNAP molecule is a collection of mass points (each mass point represents a peptide unit) and these mass points are connected by linear springs exhibiting longitudinal stretching motion parallel to the helical axis of DNA (i.e. along z direction). This longitudinal stretching motion of the RNAP molecule and its interaction with the DNA chain are represented by the Hamiltonian $H_{\mathrm{DNA-RNAP}}$:

$$H_{\mathrm{DNA-RNAP}} = \sum_n \left[\frac{q_n^2}{2m_{\mathrm{p}}} + K_{\mathrm{p}} (y_{n+1} - y_n)^2 + \alpha_2 (y_{n+1} - y_{n-1}) \left(S_n^z \cdot S_n'^z \right) \right]. \quad (12)$$

The corresponding momentum is $q_n = m_{\mathrm{p}} \dot{y}_n$.

In the Hamiltonian (12), the coordinate y_n represents displacement of the n-th peptide in the RNAP chain from its equilibrium position. The parameters m_{p}, K_{p}, and α_2 represent the peptide's mass, the elastic constant of the springs, and the linear-coupling coefficient between peptides and nucleotides, respectively. The RNAP molecule is assumed to slide on the DNA chain and the interaction energy along z direction is expected to be dominant over the energy in the xy-plane normal to it.

All these elucidations allow us to write the total Hamiltonian of our model as:

$$\begin{aligned} H &= H_{\mathrm{DNA1}} + H_{\mathrm{DNA2}} + H_{\mathrm{DNA3}} + H_{\mathrm{DNA-Phonon}} + H_{\mathrm{DNA-RNAP}} \\ &= \sum_n \Bigg[- \sum_{m>n} \Omega_{m,n} \left(S_n \cdot S_m + S_n' \cdot S_m' \right) - g(S_n' S_{n+h} + S_n S_{n+h}') \\ &\quad - \beta \left(S_n \cdot S_n' \right) + \frac{p_n^2}{2m_{\mathrm{H}}} + \frac{q_n^2}{2m_{\mathrm{p}}} \\ &\quad + \mathbf{K}_{\mathrm{H}} (x_{n+1} - x_n)^2 + K_{\mathrm{p}} (y_{n+1} - y_n)^2 \\ &\quad + \alpha_1 (x_{n+1} - x_{n-1}) \left(S_n \cdot S_n' \right) \\ &\quad + \alpha_2 (y_{n+1} - y_{n-1}) \left(S_n^z \cdot S_n'^z \right) \Bigg]. \end{aligned} \quad (13)$$

The numerical values of the model parameters are those used in Refs. [38], [44]–[51]. We usually use a classical approach or semi-classical approximation to understand the spin dynamics when the spin value is large in the case of Heisenberg spin systems.[25,52] To bosonize the Hamiltonian (13), we first consider the following two operators:

$$S_n^+ = S_n^x + \mathrm{i} S_n^y, \quad (14)$$

$$S_n^- = S_n^x - \mathrm{i} S_n^y, \quad (15)$$

and then introduce the Holstein–Primakoff representation previously transformed by Nguenang and Kofané[53–55]

$$S_n^+ = (2)^{1/2} \varepsilon \left(1 - \varepsilon^2 a_n^\dagger a_n \right)^{1/2} a_n, \quad (16)$$

$$S_n^- = (2)^{1/2} \varepsilon a_n^\dagger \left(1 - \varepsilon^2 a_n^\dagger a_n \right)^{1/2}, \quad (17)$$

$$S_n^z = 1 - \varepsilon^2 a_n^\dagger a_n. \quad (18)$$

The quantities $a_n^\dagger$ and a_n are creation and annihilation operators related to strand R, respectively. If we set $a_n'^\dagger$ and a_n', the similar operators related to strand R', similar expressions of $S_n'^+$, $S_n'^-$, and $S_n'^z$, can be written in terms of $a_n'^\dagger$ and a_n'. These creation and annihilation operators satisfy the commutation relations

$$[a_m, a_n^\dagger] = [a_m', a_n'^\dagger] = \delta_{mn}, \quad (19)$$

$$[a_m, a_n] = [a_m', a_n'] = [a_m^\dagger, a_n^\dagger] = [a_m'^\dagger, a_n'^\dagger] = 0, \quad (20)$$

where δ_{mn} is the Dirac function.

It is necessary to expand the Holstein–Primakoff representation in a power series in terms of the parameter $\varepsilon = (S)^{-1/2}$, in the low-temperature limit, i.e., $a_n^\dagger a_n \ll 2S$,

$$S_n^+ = (2)^{1/2} \varepsilon \left[1 - \frac{\varepsilon^2}{4} a_n^\dagger a_n - \frac{\varepsilon^4}{32} a_n^\dagger a_n a_n^\dagger a_n - O\left(\varepsilon^6\right) \right] a_n, \quad (21)$$

$$S_n^- = (2)^{1/2} \varepsilon a_n^\dagger \left[1 - \frac{\varepsilon^2}{4} a_n^\dagger a_n - \frac{\varepsilon^4}{32} a_n^\dagger a_n a_n^\dagger a_n - O\left(\varepsilon^6\right) \right]. \quad (22)$$

From all these considerations, the Hamiltonian (13) can be rewritten up to $O(\varepsilon^2)$ as:

$$\begin{aligned} H &= \sum_n \Bigg\{ \frac{p_n^2}{2m_{\mathrm{H}}} + \frac{q_n^2}{2m_{\mathrm{p}}} + \boldsymbol{K}_{\mathrm{H}} (x_{n+1} - x_n)^2 + K_{\mathrm{p}} (y_{n+1} - y_n)^2 \\ &\quad - [\beta - \alpha_1 (x_{n+1} - x_{n-1}) - \alpha_2 (y_{n+1} - y_{n-1})] \\ &\quad + \varepsilon^2 \Bigg[- \sum_{m>n} \Omega_{m,n} (a_n a_m^\dagger + a_n^\dagger a_m - a_n^\dagger a_n - a_m^\dagger a_m \\ &\quad + a_n' a_m'^+ + a_n'^\dagger a_m' - a_n'^\dagger a_n' - a_m'^+ a_m') \\ &\quad - g (a_n' a_{n+h}^+ + a_n'^+ a_{n+h} + a_n a_{n+h}'^\dagger + a_n^\dagger a_{n+h}' \\ &\quad - a_{n+h}^\dagger a_{n+h} - a_{n+h}'^\dagger a_{n+h}' \\ &\quad - a_n^\dagger a_n - a_n'^\dagger a_n') - 2g - 2 \sum_{m>n} \Omega_{m,n} \\ &\quad - (\beta - \alpha_1 (x_{n+1} - x_{n-1})) (a_n^\dagger a_n' + a_n a_n'^\dagger - a_n^\dagger a_n - a_n'^\dagger a_n') \\ &\quad - \alpha_2 (y_{n+1} - y_{n-1}) (a_n^\dagger a_n + a_n'^\dagger a_n') \Bigg] \Bigg\}. \end{aligned} \quad (23)$$

In the next section, we will use the above Hamiltonian to derive the equations of motion for a base, a peptide, and a hydrogen atom.

3. Dynamical equations

The equations for the bosonic operators $a_n^\dagger$, a_n, $a_n'^\dagger$, and a_n' can be obtained in the Heisenberg picture by introducing the Hamiltonian (23) in the equations

$$\mathrm{i}\hbar \dot{a}_n = [a_n, H], \quad \mathrm{i}\hbar \dot{a}_n' = [a_n', H], \quad (24)$$

where $\hbar$ is the reduced Planck constant, the dot denotes $\partial/\partial t$ and the i situated in front of operators is imaginary number, i.e., $\mathrm{i}^2 = -1$.

The equations of motion for hydrogen atom and peptide can be obtained using Hamilton's equations

$$\partial p_n / \partial t = -\partial H / \partial x_n, \quad \partial x_n / \partial t = \partial H / \partial p_n,$$

$$\partial q_n/\partial t = -\partial H/\partial y_n, \quad \partial y_n/\partial t = \partial H/\partial q_n. \tag{25}$$

Thus, the whole system is described by the set of equations

$$\begin{aligned}
\mathrm{i}\hbar\dot{a}_n &= \varepsilon^2\Big\{-\sum_{m\neq n}\Omega_{m,n}(a_m-a_n)-g(a'_{n+h}+a'_{n-h}-2a_n)\\
&\quad-[\beta-\alpha_1(x_{n+1}-x_{n-1})](a'_n-a_n)\\
&\quad-\alpha_2(y_{n+1}-y_{n-1})a_n\Big\}, \qquad (26)\\
\mathrm{i}\hbar\dot{a}'_n &= \varepsilon^2\Big\{-\sum_{m\neq n}\Omega_{m,n}(a'_m-a'_n)-g(a_{n+h}+a_{n-h}-2a'_n)\\
&\quad-[\beta-\alpha_1(x_{n+1}-x_{n-1})](a_n-a'_n)\\
&\quad-\alpha_2(y_{n+1}-y_{n-1})a'_n\Big\}, \qquad (27)\\
m_{\mathrm{H}}\ddot{x}_n &= 2\boldsymbol{K}_{\mathrm{H}}(x_{n+1}+x_{n-1}-2x_n)-\varepsilon^2\alpha_1(a^{\dagger}_{n-1}a_{n-1}+a'^{+}_{n-1}a'_{n-1}\\
&\quad-a^{\dagger}_{n+1}a_{n+1}-a'^{\dagger}_{n+1}a'_{n+1}+a^{\dagger}_{n+1}a'_{n+1}\\
&\quad+a_{n+1}a'^{+}_{n+1}-a^{\dagger}_{n-1}a'_{n-1}-a_{n-1}a'^{+}_{n-1}), \qquad (28)\\
m_{\mathrm{p}}\ddot{y}_n &= 2K_{\mathrm{p}}(y_{n+1}+y_{n-1}-2y_n)-\varepsilon^2\alpha_2(a^{\dagger}_{n-1}a_{n-1}\\
&\quad+a'^{+}_{n-1}a'_{n-1}-a^{\dagger}_{n+1}a_{n+1}-a'^{+}_{n+1}a'_{n+1}). \qquad (29)
\end{aligned}$$

By using Glauber's coherent state representation[56] for boson operators, $a^{\dagger}_n \mid f\rangle = f^*_n \mid f\rangle$, $a_n \mid f\rangle = f_n \mid f\rangle$, $\mid f\rangle = \sum_n \mid f_n\rangle$, $a'^{\dagger}_n \mid f'\rangle = f'^*_n \mid f'\rangle$, $a'_n \mid f'\rangle = f'_n \mid f'\rangle$, $\mid f'\rangle = \sum_n \mid f'_n\rangle$, $\langle f \mid f\rangle = 1$, and $\langle f' \mid f'\rangle = 1$, the above set of equations becomes:

$$\begin{aligned}
\mathrm{i}\hbar\dot{f}_n &= \varepsilon^2\Big\{-\sum_{m\neq n}\Omega_{m,n}(f_m-f_n)-g(f'_{n+h}+f'_{n-h}-2f_n)\\
&\quad-[\beta-\alpha_1(x_{n+1}-x_{n-1})](f'_n-f_n)\\
&\quad-\alpha_2(y_{n+1}-y_{n-1})f_n\Big\}, \qquad (30)\\
\mathrm{i}\hbar\dot{f}'_n &= \varepsilon^2\Big\{-\sum_{m\neq n}\Omega_{m,n}(f'_m-f'_n)-g(f_{n+h}+f_{n-h}-2f'_n)\\
&\quad-[\beta-\alpha_1(x_{n+1}-x_{n-1})](f_n-f'_n)\\
&\quad-\alpha_2(y_{n+1}-y_{n-1})f'_n\Big\}, \qquad (31)\\
m_{\mathrm{H}}\ddot{x}_n &= 2\boldsymbol{K}_{\mathrm{H}}(x_{n+1}+x_{n-1}-2x_n)-\varepsilon^2\alpha_1(|f_{n-1}|^2+|f'_{n-1}|^2\\
&\quad-|f_{n+1}|^2-|f'_{n+1}|^2+f^*_{n+1}f'_{n+1}\\
&\quad+f_{n+1}f'^*_{n+1}-f^*_{n-1}f'_{n-1}-f_{n-1}f'^*_{n-1}), \qquad (32)\\
m_{\mathrm{p}}\ddot{y}_n &= 2K_{\mathrm{p}}(y_{n+1}+y_{n-1}-2y_n)\\
&\quad-\varepsilon^2\alpha_2(|f_{n-1}|^2+|f'_{n-1}|^2-|f_{n+1}|^2-|f'_{n+1}|^2), \qquad (33)
\end{aligned}$$

where f_n and f'_n are the coherent amplitudes of the operators a_n and a'_n, respectively. We have also considered that the system is in the states $\mid f\rangle$ and $\mid f'\rangle$ for the operators a_n and a'_n, respectively.

During the opening of the DNA's strands, the complementary bases to the same base pair move in the opposite directions and then we can take $f'_n = -f_n$. The set of Eqs. (30)–(33) leads to

$$\begin{aligned}
\mathrm{i}\hbar\dot{f}_n &= \varepsilon^2\Big\{-\sum_{m\neq n}\Omega_{m,n}(f_m-f_n)+g(f_{n+h}+f_{n-h}+2f_n)\\
&\quad-[2\alpha_1(x_{n+1}-x_{n-1})\\
&\quad+\alpha_2(y_{n+1}-y_{n-1})-2\beta]f_n\Big\}, \qquad (34)\\
m_{\mathrm{H}}\ddot{x}_n &= 2\boldsymbol{K}_{\mathrm{H}}(x_{n+1}+x_{n-1}-2x_n)\\
&\quad+4\varepsilon^2\alpha_1(|f_{n-1}|^2-|f_{n+1}|^2), \qquad (35)\\
m_{\mathrm{p}}\ddot{y}_n &= 2K_{\mathrm{p}}(y_{n+1}+y_{n-1}-2y_n)\\
&\quad+2\varepsilon^2\alpha_2(|f_{n-1}|^2-|f_{n+1}|^2). \qquad (36)
\end{aligned}$$

We note $\lambda = m-n$, and Eq. (34) becomes

$$\begin{aligned}
\mathrm{i}\hbar\dot{f}_n &= \varepsilon^2\Big\{-\frac{1}{2}\sum_{\lambda=1}^{\infty}\frac{\Omega(f_{n+\lambda}+f_{n-\lambda}-2f_n)}{|\lambda|^{\mathbf{r}}}\\
&\quad+g(f_{n+h}+f_{n-h}+2f_n)\\
&\quad-[2\alpha_1(x_{n+1}-x_{n-1})\\
&\quad+\alpha_2(y_{n+1}-y_{n-1})-2\beta]f_n\Big\}. \qquad (37)
\end{aligned}$$

To obtain the analytic localized solutions of the similar discrete NLS equation with LRI, Rasmussen *et al.*[57] used the variational method. In this work, we used the Taylor series expansion to reproduce the similar exponential localized solutions. It is known that in the nonlinear problems, the complexity of studies can depend on the mathematical order of the derivative during Taylor series expansion. The precision of results increases with the orders of derivatives. For this reason, we first consider the short order derivative to study the effects of LRI and HC on the DNA dynamics, and afterwards increase the order of expansion to know if the results are modified.

4. Results for the second-order terms in a Taylor expansion

In this case, we go to the continuum limit by using the following approximation: $nd \to z$, $f_n \to f(z,t)$, $x_n \to x(z,t)$, $y_n \to y(z,t)$, and then, expand the terms of $f_{n\pm\lambda}$, $y_{n\pm1}$, and $x_{n\pm1}$ in Taylor series as

$$\begin{aligned}
f_{n\pm\lambda} &= \sum_{l=0}^{\infty}\frac{(d\lambda)^l}{l!}\frac{\partial^l f}{\partial z^l}, \quad y_{n\pm1} = \sum_{l=0}^{\infty}\frac{d^l}{l!}\frac{\partial^l y}{\partial z^l},\\
x_{n\pm1} &= \sum_{l=0}^{\infty}\frac{d^l}{l!}\frac{\partial^l x}{\partial z^l}, \qquad (38)
\end{aligned}$$

where d is the distance between consecutive bases (or peptides) in the same strand.

Introducing these expansions in set of Eqs. (34)–(36), we easily obtain the following equations after rescaling $z \to z/d$ and considering space up to $O(d^2)$

$$\mathrm{i}f_t = -[\Omega\ \zeta(\boldsymbol{r}-2)-gh^2]f_{zz}$$

$$-[2\alpha_1 x_z + \alpha_2\, y_z - 2\beta - 4g]f, \tag{39}$$

$$m_{\rm H} x_{tt} = K_{\rm H} x_{zz} - 4\alpha_1 (|f|^2)_z, \tag{40}$$

$$m_{\rm p} y_{tt} = K_{\rm p} y_{zz} - 2\alpha_2 (|f|^2)_z. \tag{41}$$

While writing the above equations of motion Eqs. (39)–(41), parameters α_1, α_2, β, Ω, $K_{\rm H}$, g, and $K_{\rm p}$ are dimensionless.

To simplify our equations, we first derive Eqs. (40) and (41) with respect to z once and define a new variable $s = z - v_{\rm g}t$, where $v_{\rm g}$ is the group velocity of the wave in the system. These equations give

$$x_{sss} = [4\alpha_1/m_{\rm H}(v_1^2 - v_{\rm g}^2)](|f|^2)_{ss}, \tag{42}$$

$$y_{sss} = [2\alpha_2/m_{\rm p}(v_2^2 - v_{\rm g}^2)](|f|^2)_{ss}. \tag{43}$$

The quantities $v_1^2 = K_{\rm H}/m_{\rm H}$ and $v_2^2 = K_{\rm p}/m_{\rm p}$ are the square of the sound's velocities in the phonon network and in the RNAP molecule, respectively. Note that as DNA is a dispersive system, the group velocity $v_{\rm g}$ can be obtained from the dispersion relation.[41,42,58] By integrating two times Eqs. (42) and (43) with respect to s and annulling the integration constants, we get the following set of equations after reconsidering z

$$\begin{aligned} {\rm i}f_t &= -[\Omega\ \zeta(r-2) - gh^2]f_{zz} \\ &\quad -[8\alpha_1\eta_1 + 4\alpha_2\eta_2]|f|^2 f\ + (2\beta + 4g)f, \end{aligned} \tag{44}$$

$$x_z = 2\eta_1 |f|^2, \tag{45}$$

$$y_z = 2\eta_2 |f|^2, \tag{46}$$

where $\eta_1 = 2\alpha_1/m_{\rm H}(v_1^2 - v_{\rm g}^2)$ and $\eta_2 = \alpha_2/m_{\rm p}(v_2^2 - v_{\rm g}^2)$.

Since our purpose is to study the behavior of a DNA molecule when an RNAP molecule binds to it, we focus our attention on Eq. (44). In this equation, the nonlinearity is brought by the RNAP binding, and the coupling of the thermal phonons in the DNA strand, respectively, while the dispersion is brought by the intra-strand coupling and HC, respectively. It can be moderated by using a gauge transformation $F(z,t) = f(z,t)\,{\rm e}^{{\rm i}(2\beta+4g)t}$. Then, Eq. (44) is rewritten as

$${\rm i}F_t + PF_{zz} + Q|F|^2 F = 0 \tag{47}$$

with

$$Q = 4(2\alpha_1\eta_1 + \alpha_2\eta_2), \tag{48}$$

$$P = \Omega\zeta(r-2) - gh^2. \tag{49}$$

Equation (47) is the well-known completely integrable NLS equation, which describes a DNA strand's dynamics during the process of transcription, induced by an RNAP molecule at the physiological temperature. It can be checked that when $r \to \infty$ (nearest-neighbor interaction) and ignoring the helicoidal structure of the DNA molecule, this equation is reduced to the NLS equation obtained by Vasumathi and Daniel.[25] In spite of us considering the second-order terms in the Taylor expansion, the coefficients of the obtained NLS equation depend on the LRI parameter. One can consider that this is the case of quasi LRI between nucleotides.

4.1. Dispersion relation for DNA linear dynamics

We first note that ignoring the effect of the thermal fluctuation and considering a situation in which the RNAP has not interacted with the DNA, the nonlinear term disappears in Eq. (47). In this situation, the DNA dynamics is governed by the plane transverse wave of the form

$$F = B_0 \exp[{\rm i}(qz - \omega t)], \tag{50}$$

which yields the dispersion relation

$$\omega = q^2(\Omega\zeta(r-2) - gh^2). \tag{51}$$

The quantities B_0, q, and ω are the constant amplitude, the wave vector, and the frequency, respectively. We deduce the group velocity

$$v_{\rm g} = 2(\Omega\zeta(r-2) - gh^2)q, \tag{52}$$

and note that both the group velocity and the dispersion relation are influenced by the HC constant g and by the LRI parameter r. The condition $\zeta(r-2)/g > h^2/\Omega$ is required for a positive group velocity. We should note that $v_{\rm g}$ increases with the decreasing of the long range parameter r, and becomes infinite at $r = 3$. A similar expression of group velocity was obtained by Mingaleev *et al.*[39] when studying the effects of the power-law LRI on the properties of soliton excitations in anharmonic chains. They showed the suitability to take $r > 3$ for the existence of solitonic waves in the system. They also suggested that their study could be applied to the DNA dynamics. For this reason, we restrict ourselves to the case $r > 3$ for what follows in this paper. LRI and HC are responsible for quite relevant changes in the free DNA dynamics as plotted in Fig. 2, which presents different features of the dispersion relation for various values of LRI parameter and HC constant. In this figure, we note from the behavior of the frequency that the wave's dispersion decreases with the increasing of each of these two parameters. From Fig. 2(a), the frequency of the DNA linear dynamics becomes negative for $\Omega\zeta(r-2) < gh^2$. Then, this unphysical behavior of the linear dispersion arises when the HC force is more important than the intra-strand coupling force.

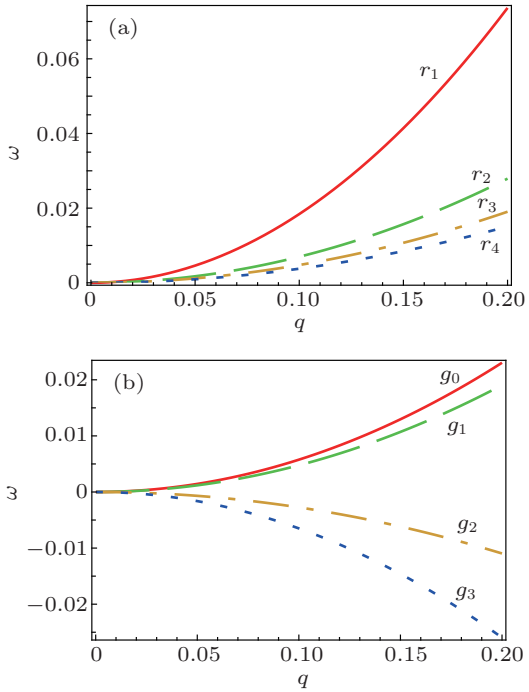


Fig. 2. (color online) Dispersion relation curves: ω as a function of q for different values of r (a) with $g = 0.015$, $r_1 = 3.3$, $r_2 = 4$, $r_3 = 5$, $r_4 = 10$, and (b) with $r = 4$, $g_0 = 0.0$, $g_1 = 0.02$, $g_2 = 0.04$, $g_3 = 0.05$. One can note that ω is a decreasing function of r and g.

4.2. Solitonic-like wave solution analysis

Now, let us turn our attention to the full nonlinear equation (see Eq. (47)), i.e., the case where RNAP binds to the promoter site of the DNA molecule at the biological temperature. As is well known, the solutions of the NLS equation depend on the signs of the dispersive and nonlinear coefficients. The coefficient $Q > 0$ since $v_1 \geq v_g$ and $v_2 \geq v_g$ (see Ref. [25]). The dispersive coefficient $P < 0$ for $g/\zeta(r-2) > \Omega/h^2$. In this case, the product $PQ < 0$, the solutions of the NLS equation are envelope hole waves where the depression of an envelope propagates as a soliton with a finite amplitude at $|z| \to \infty$. These waves are also called dark-solitons. For $0 \leq g < \Omega\zeta(r-2)/h^2$, $P > 0$ and then $PQ > 0$. In this case, the solutions of the NLS equation are localized envelope solitons (or breather-like solutions), which have a vanishing amplitude at $|z| \to \infty$. It has been proved by the studies, supported by the numerical simulations that such a localized envelope soliton has the appropriate shape to represent RNAP-DNA dynamics.[7,25] Then, in the real DNA helicoidal structure,

$$0 \leq g < g_{\max} \quad \text{with} \quad g_{\max} = \frac{\Omega\zeta(r-2)}{h^2}. \tag{53}$$

This means that the HC is weak compared to intra-strand coupling in the real DNA molecule.

The area in which one could expect a localized envelope solution of Eq. (47), according to r and g, is represented in Fig. 3, as given by Eq. (53). This area depends strongly on LRI and HC parameters. Let us now give an explicit expression of this solitonic wave under the above conditions. For $PQ > 0$ the localized envelope soliton solution of Eq. (47) is given by[59,60]

$$F(z,t) = F_0 \,\mathrm{sech}[(1/L_e)(z - v_e t) + A_0] \times \exp\left[\mathrm{i}\frac{v_e}{2P}(z - v_c t) + \theta_0\right], \tag{54}$$

where F_0 is given by

$$F_0 = [(v_e^2 - 2v_c v_e)/2PQ]^{1/2}, \tag{55}$$

and

$$L_e = \frac{2P}{\sqrt{v_e^2 - 2v_c v_e}}. \tag{56}$$

The parameters A_0 and θ_0 are initial position and initial phase, respectively. The quantity $v_e^2 - 2v_c v_e > 0$ for DNA dynamics,[59] where v_e and v_c are positive velocities of the envelope and the carrier waves, respectively. For simplification, it is convenient to introduce as in Ref. [61] a new parameter $\boldsymbol{\mu}$ defined through

$$v_c = \boldsymbol{\mu} v_e \quad \text{with } \boldsymbol{\mu} \in [0; 0.5]. \tag{57}$$

Since the wave is modulated if $\boldsymbol{\mu}$ is close to its limit 0.5, the parameter $\boldsymbol{\mu}$ represents a measure for modulation. The parameter L_e is the width of the breather.

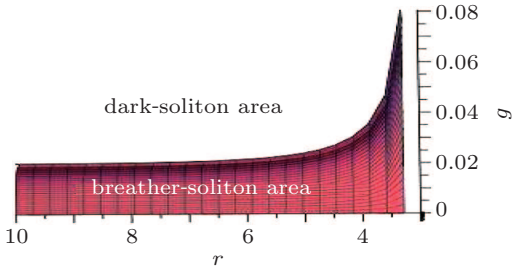


Fig. 3. (color online) Breather-like solitonic wave area.

Introducing Eqs. (48), (49), and (57) in Eqs. (54), (55), and (56), we can write

$$F(z,t) = \left(\frac{v_e}{2}\sqrt{\frac{1-2\boldsymbol{\mu}}{2(\Omega\zeta(r-2) - gh^2)(2\alpha_1\eta_1 + \alpha_2\eta_2)}}\right) \times \mathrm{sech}\left[\frac{v_e\sqrt{1-2\boldsymbol{\mu}}}{2(\Omega\zeta(r-2) - gh^2)}(z - v_e t) + A_0\right] \times \exp \mathrm{i}\left[\frac{v_e}{2(\Omega\zeta(r-2) - gh^2)}(z - \boldsymbol{\mu} v_e t) + \theta_0\right]. \tag{58}$$

and

$$L_e = \frac{2(\Omega\zeta(r-2) - gh^2)}{v_e\sqrt{1-2\boldsymbol{\mu}}}. \tag{59}$$

Using Eq. (58), we obtain the expression of $f(z,t)$

$$f(z,t) = \left(\frac{v_e}{2}\sqrt{\frac{1-2\boldsymbol{\mu}}{2(\Omega\zeta(r-2) - gh^2)(2\alpha_1\eta_1 + \alpha_2\eta_2)}}\right) \times \mathrm{sech}\left[\frac{v_e\sqrt{1-2\boldsymbol{\mu}}}{2(\Omega\zeta(r-2) - gh^2)}(z - v_e t) + A_0\right]$$

$$\times \exp \mathrm{i}\left[\frac{v_\mathrm{e}}{2(\Omega\zeta(r-2)-gh^2)}z - \left(\frac{\mu v_\mathrm{e}^2}{2(\Omega\zeta(r-2)-gh^2)}+2\beta+4g\right)t+\theta_0\right], \quad (60)$$

and deduce the expression of the wave in the complementary strand R', $f'(z,t) = -f(z,t)$

$$\begin{aligned} f'(z,t) = & -\left(\frac{v_\mathrm{e}}{2}\sqrt{\frac{1-2\mu}{2(\Omega\zeta(r-2)-gh^2)(2\alpha_1\eta_1+\alpha_2\eta_2)}}\right) \\ & \times \operatorname{sech}\left[\frac{v_\mathrm{e}\sqrt{1-2\mu}}{2(\Omega\zeta(r-2)-gh^2)}(z-v_\mathrm{e}t)+A_0\right] \\ & \times \exp \mathrm{i}\left[\frac{v_\mathrm{e}}{2(\Omega\zeta(r-2)-gh^2)}(z-\mu v_\mathrm{e}t)\right. \\ & \left.-(2\beta+4g)t+\theta_0\right]. \end{aligned} \quad (61)$$

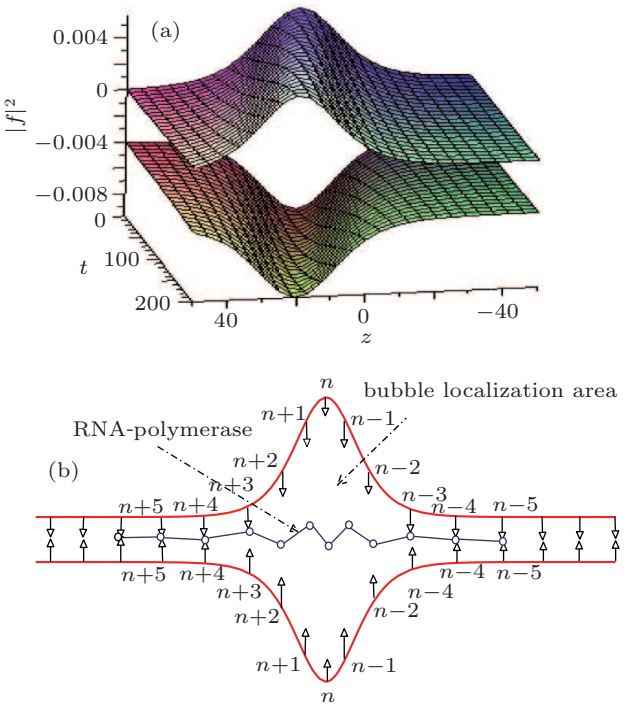


Fig. 4. (color online) (a) Three-dimensional (3D) representation of the DNA strands during the transcription process, (b) representation of the DNA promoter site when RNAP is bound on it at biological temperature. The strands have been plotted numerically and the RNAP molecule has been added schematically. The arrows illustrate the hydrogen bonds between complementary bases.

These envelope solitons as plotted in Fig. 4(a), represent the opening of base pairs in both strands. We note that the breather-like soliton moves along these strands with time evolving. Indeed, when an RNAP molecule nears the promoter site of the DNA molecule at the biological temperature, it excites the bases lying on this site. The energy of these bases increases and the nonlinearity localizes it. Then, the interplay between nonlinear and dispersive effects, resulting from these excitations, generates localized mode in each strand. The formation of these breather-like solitons in both strands is done in the opposite transverse directions and thus, collectively forms a bubble. When the RNAP molecule moves along the DNA chain, it carries away the bubble with it. Then, as a zip runner, the RNAP is the instigator of the bubble in the promoter site of the DNA. That bubble moves along the DNA molecule (see Fig. 4(a)), causing the opening of the complementary strands by separating the adjacent bases. This phenomenon is the denaturation of the DNA macromolecule. We have numerically plotted the two DNA strands in Fig. 4(b), and have schematically added the RNAP molecule and the arrows which represent the hydrogen bonds between complementary bases.

4.3. Impact of LRI and HC on bubble sizes

From the expression for the bubble (see Eqs. (59)–(61)), for the solution of the NLS equation (see Eq. (47)), it is understood that all its characteristics (phase, amplitude, and width) depend on the LRI parameter r through Riemann zeta function and on the HC parameter g. Thus, it is clear that the power

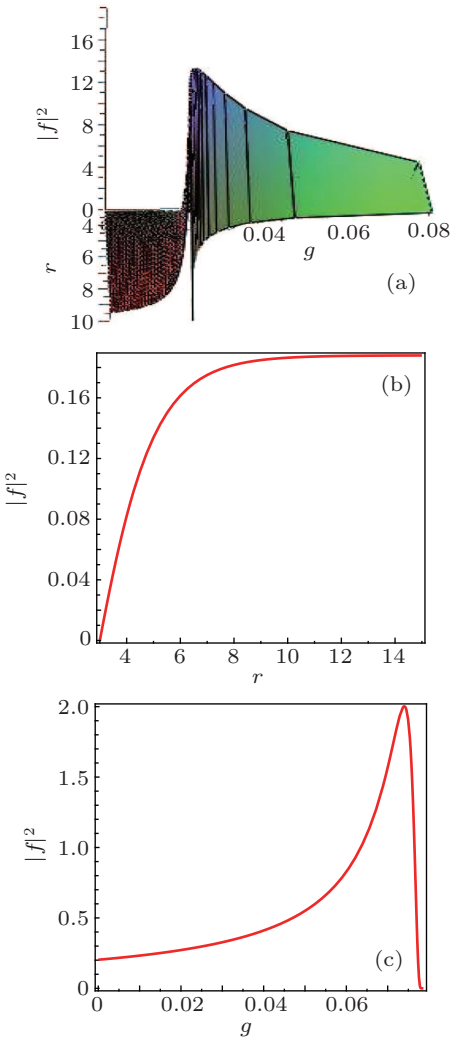


Fig. 5. (color online) (a) The 3D schematic feature of the square of the envelope soliton according to LRI and HC parameters, (b) evolution of the square of the bubble height as a function of LRI parameter. We note that the height of the bubble increases with the increasing of r. (c) The bearing of the HC on the square of the bubble height. One can note that the bubble exists even if the HC is disregarded (i.e., $g = 0$).

law LRI and HC affect deeply the unzipping process of the DNA molecule at the physiological temperature. As shown in Fig. 5(a), the amplitude of the bubble is a function of both parameters.

These influences are clearly illustrated in Figs. 5(b) and 5(c). Figure 5(b) shows that the square of the amplitude of the bubble increases rapidly with the increasing of r (when r nears 3), but becomes insensitive when r is large. This means that the height of the breather in the nearest neighbor interaction is less sensitive than the one in the infinite neighbor interaction. In other words, the breather's height is constant if a base interacts only with its close neighbors, but if a base pair interacts with many other pairs, the height of the breather decreases with the number of pairs which influence its dynamics. One can see from Fig. 5(c) that when g increases, the energy of the bubble increases and after reaches its peak for a critical value $g_{\rm cr}$ of g, this square of the amplitude of the bubble decreases very rapidly and is reduced to zero for $g = g_{\max}$. Analytical calculus have shown that the critical value $g_{\rm cr}$ of g verifies the relation

$$\tanh\left[\frac{v_{\rm e}\sqrt{1-2\mu}}{2(\Omega\zeta(r-2)-g_{\rm cr}h^2)}(z-v_{\rm e}t)+A_0\right] = \left[\frac{v_{\rm e}\sqrt{1-2\mu}}{(\Omega\zeta(r-2)-g_{\rm cr}h^2)}(z-v_{\rm e}t)+A_0\right]^{-1}. \quad (62)$$

We also note from this figure that the bubble exists even if the HC is disregarded. Indeed, the square of the absolute value of the bubble is not null for $g = 0$. This result is in agreement with earlier studies which have been done without taking into account the HC and interesting results have been obtained.[25,62] To give more elucidations of the effect of LRI and HC on bubble sizes during the transcription phenomenon, we have plotted the feature of our solution for different values of the LRI parameter and HC constant in Figs. 6(a) and 6(b), respectively. For four values of LRI parameter $r_1 = 3.3$, $r_2 = 4$, $r_3 = 5$, and $r_4 = 10$, and four values of HC constant $g_0 = 0$, $g_1 = (1/4)g_{\max}$, $g_2 = (1/2)g_{\max}$, and $g_3 = (3/4)g_{\max}$, these figures reveal not only that the bubble's height increases with the increasing of the LRI's parameter and with the increasing of the HC constant, but show also that the number of base pairs that are disrupted and participate in the unzipping process depends on r and g. Indeed, we note that the number of base pairs which form the bubble decreases with the increasing of both r and g. This means that the width of the bubble (or the number of base pairs which form the bubble) increases if a base pair interacts with many other pairs, on the one hand, and that a strong HC reduces the number of base pairs which form the bubble, on the other hand. In other words, strong HC coupling or weak LRI between nucleotides leads to a highly localized longitudinal wave with high amplitude which can be used to better describe the unzipping of DNA, while weak HC or strong LRI between nucleotides leads to a small amplitude localized longitudinal wave with large spatial expansion which can be used to explain data transfer in the DNA. For more precision, when the HC is ignored, about 16 base pairs which form the bubble are reduced to approximately 8 base pairs for $g = g_3$ (see Fig. 6(b)), and about 17 base pairs which form that bubble when $r = r_1$ are reduced to approximately 7 base pairs for $r = r_4$ (see Fig. 6(a)). This result does not disagree with experimental ones. Indeed, at the physiological temperature, Wang *et al.*[63] studied through gel electrophoresis the unwinding of the DNA helix when an RNAP binds to it in a medium having the characteristics of the environment in which DNA works. They found by measuring that the unwinding angle of the DNA per bound enzyme is 140 °C, and that the total unwinding angle for a fixed number of bound polymerase molecules per DNA decreases with decreasing temperature. Using UV absorption spectroscopy, Hsieht *et al.*[64] studied the interaction between an RNAP and a fragment of DNA containing four promoter sites. The temperature in this study was in the range 4 °C–140 °C. They found that the binding of an RNAP to a promoter site in the low ionic strength medium causes the disruption of a short segment of the DNA helix, of the order of ten pairs. Melnikova *et al.*[65] using the dimethylsulphate method found that enzymes can break until 15 Watson–Crick base-pairings in a DNA molecule. Siebenlist[66] used radiogram measurements at the physiological temperature to identify the exact region that RNAP opens in the A3 promoter of

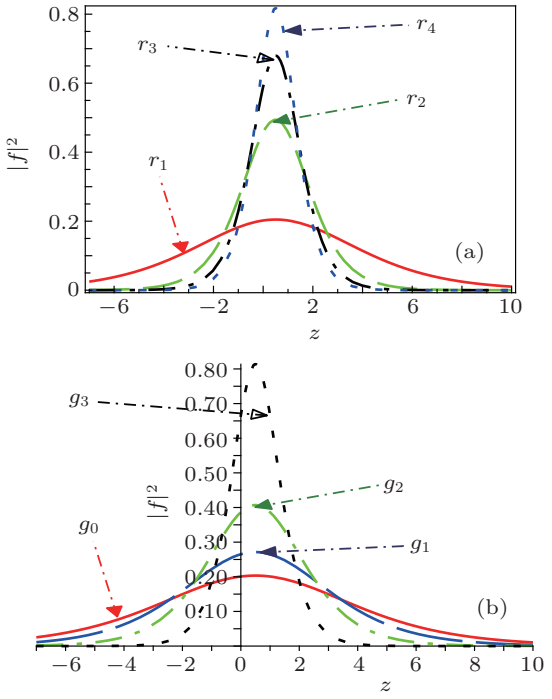


Fig. 6. (color online) Breather-like soliton profiles for various values of (a) LRI parameter r for $g = 0.01$, $r_1 = 3.3$, $r_2 = 4$, $r_3 = 5$, and $r_4 = 10$; (b) HC constant g for $r = 5$, $g_0 = 0.0$, $g_1 = (1/4)g_{\max}$, $g_2 = (1/2)g_{\max}$, $g_3 = (3/4)g_{\max}$. We note that the width of the bubble decreases with the increasing of both r and g.

phage T7, and its results agree with those of the above three experimental works, that the bubble is formed by around 7 to 15 base pairs. The results obtained in the present study are within that range. This coincidence proves the truth of our model to describe the base pairs opening.

5. Results for the fourth-order terms in a Taylor expansion

In the present case, we reconsider Eq. (37) and go to the continuum limit by adding the following approximation in those of Eq. (38), $f_{n+\lambda} = \mathrm{e}^{\lambda\partial_z} f(z,t)$.[67] Afterwards, we define operator[39]

$$W(r,\partial_z) = 2\sum_{\lambda=0}^{\infty} \frac{1-\cosh(\lambda\partial_z)}{\lambda^r}.$$

With this procedure, the equivalence of Eq. (44) is given by

$$\begin{aligned} \mathrm{i}f_t \;=\; & \Omega\, W(r,\partial_z)f + gh^2 f_{zz} \\ & -4[2\alpha_1\eta_1+\alpha_2\eta_2]|f|^2 f + (2\beta+4g)f. \end{aligned} \tag{63}$$

Operator $W(r,\partial_z)$ is usually expressed in the long wave limit as follows:[39,68]

$$W(r,\mathrm{i}b) \;\approx\; \zeta(r-2)b^2 - \frac{1}{12}\zeta(r-4)b^4 \quad \text{for } r>5, \tag{64}$$

$$W(5,\mathrm{i}b) \;\approx\; \zeta(3)b^2 + \frac{1}{12}b^4\ln|b|, \tag{65}$$

$$\begin{aligned} W(r,\mathrm{i}b) \;\approx\; & \zeta(r-2)b^2 - v_r|b|^{r-1} + \frac{r-3}{24(5-r)}b^4 \\ & \text{for} \quad 5>r \quad >3, \end{aligned} \tag{66}$$

$$W(4,\mathrm{i}b) \;\approx\; \frac{\pi^2}{6}b^2 - \frac{\pi}{6}|b|^3 + \frac{1}{24}b^4, \tag{67}$$

$$W(3,\mathrm{i}b) \;\approx\; -b^2\ln|b| + \frac{3}{2}b^2 + \frac{1}{144}b^4, \tag{68}$$

where

$$v_r = \frac{2^{1-r}\pi^{3/2}}{\Gamma(s/2)\Gamma((r+1)/2)\cos(\pi r/2)},$$

Γ is the gamma function. Using the transformation $F(z,t) = f(z,t)\,\mathrm{e}^{\mathrm{i}(2\beta+4g)t}$, the form of the equation describing the DNA dynamics then depends on the long-range parameter as follows:

$$\mathrm{i}F_t + B_1F_{zz} + B_2|F|^2F = B_3F_{zzzz} \quad \text{for } r>5; \tag{69}$$

$$\begin{aligned} & \mathrm{i}F_t + B_4F_{zz} + B_2|F|^2F = B_5[\partial_{zzzz}\ln(|-\mathrm{i}F_z|)] \\ & \text{for } r=5; \end{aligned} \tag{70}$$

$$\begin{aligned} & \mathrm{i}F_t + B_1F_{zz} + B_2|F|^2F = B_6F_{zzzz} + B_7[|-\mathrm{i}F_z|^{r-1}] \\ & \text{for } 5>r>3; \end{aligned} \tag{71}$$

$$\begin{aligned} & \mathrm{i}F_t + B_8F_{zz} + B_2|F|^2F = B_9F_{zzzz} + B_{10}(|-\mathrm{i}F_z|^3) \\ & \text{for } r=4; \end{aligned} \tag{72}$$

$$\begin{aligned} & \mathrm{i}F_t + B_{11}F_{zz} + B_2|F|^2F = B_{12}F_{zzzz} + B_{13}[\partial_{zz}\ln(|-\mathrm{i}F_z|)] \\ & \text{for } r=3. \end{aligned} \tag{73}$$

Here, $B_{1,\ldots,13}$ are constants defined by: $B_1 = \Omega\zeta(r-2) - gh^2$, $B_2 = 4(2\alpha_1\eta_1+\alpha_2\eta_2)$, $B_3 = \Omega\zeta(r-4)/12$, $B_4 = \Omega\zeta(3) - gh^2$, $B_5 = -\Omega/12$, $B_6 = \Omega(r-3)/24(r-5)$, $B_7 = \Omega v_r$, $B_8 = \Omega\pi^2/6 - gh^2$, $B_9 = -\Omega/24$, $B_{10} = \pi\Omega/6$, $B_{11} = 3\Omega/2 - gh^2$, $B_{12} = -\Omega/144$, and $B_{13} = -\Omega$.

Due to the complexity of these equations, each of them can be solved differently, depending of its form. We first consider Eq. (69), rescale the variable t as $t \to t/B_1$, and define a new other function F such as $F \to (B_1/B_2)^{1/2}F$. Then Eq. (69) is reduced to

$$\mathrm{i}F_t + F_{zz} + 2|F|^2F + \varepsilon\chi F_{zzzz} = 0, \tag{74}$$

where $\varepsilon\chi = B_3/B_1$, with ε being a small parameter. Then, we can treat the term proportional to χ as a weak perturbation. When $\varepsilon = 0$, Eq. (74) reduces to a completely integrable NLS equation, as found in Eq. (47), for which the one-soliton solution can be written as

$$F = A\,\mathrm{sech}A(\theta-\theta_0)\,\mathrm{e}^{\mathrm{i}[v(\theta-\theta_0)+(\sigma-\sigma_0)]}, \tag{75}$$

where

$$\frac{\partial\theta}{\partial t} = -2v, \quad \frac{\partial\theta}{\partial z} = 1, \quad \frac{\partial\sigma}{\partial t} = v^2+A^2, \quad \frac{\partial\theta}{\partial z} = 0.$$

The parameters A and v are related to the scattering parameter of the inverse scattering transform (IST). We now carry out a multiple scale perturbation analysis on Eq. (74) following the perturbation method of Kodama and Ablowitz[69] as done in Refs. [36] and [70]. For this, first, we introduce a slow time variable $T = \varepsilon t$ and write the quantities θ_0, A, v, and σ_0 as functions of this timescale so that the envelope soliton solution of Eq. (74) is written as $F = \hat{F}(\theta,T;\varepsilon)\,\mathrm{e}^{\mathrm{i}[v(\theta-\theta_0)+(\sigma-\sigma_0)]}$. Under the quasi-stationary assumption, Eq. (74) takes the form

$$-A^2\hat{F} + \hat{F}_{\theta\theta} + 2|\hat{F}|^2\hat{F} = \varepsilon R(\hat{F}), \tag{76}$$

where

$$\begin{aligned} R(\hat{F}) \;=\; & [v_T(\theta-\theta_0) - v\theta_{0T} - \sigma_{0T} - \chi v^4]\hat{F} - \chi\hat{F}_{\theta\theta\theta\theta} \\ & + 6v^2\chi\hat{F}_{\theta\theta} - \mathrm{i}(\hat{F}_T + 4v\chi\hat{F}_{\theta\theta\theta} - 4v^3\chi\hat{F}_\theta). \end{aligned} \tag{77}$$

Assuming Poincaré-type asymptotic expansion for $\hat{F}$

$$\hat{F}(\theta,T;\varepsilon) = \sum_{j=0}^{\infty}\varepsilon^j\hat{F}_j(\theta,T)$$

and making the first order perturbation, $\hat{F}(\theta,T;\varepsilon) = \hat{F}_0 + \varepsilon(\phi_1 + \mathrm{i}\psi_1)$ where $\hat{F}_0 = A\,\mathrm{sech}A(\theta-\theta_0)$, ϕ_1 and ψ_1 are real, we get

$$L_1\phi_1 \equiv -A^2\phi_1 + \phi_{1\theta\theta} + 6\hat{F}_0^2\phi_1 = \mathrm{Re}\,K(\hat{F}_0), \tag{78}$$

$$L_2\psi_1 \equiv -A^2\psi_1 + \psi_{1\theta\theta} + 2\hat{F}_0^2\psi_1 = \mathrm{Im}\,K(\hat{F}_0), \tag{79}$$

where L_1 and L_2 are self-adjoint operators and $\mathrm{Re}\,K(\hat{F}_0)$ and $\mathrm{Im}\,K(\hat{F}_0)$ represent the real and imaginary parts of $K(\hat{F}_0)$, given by

$$\mathrm{Re}\,K(\hat{F}_0) \;=\; [v_T(\theta-\theta_0) - v\theta_{0T} - \sigma_{0T} - \chi v^4]\hat{F}_0$$

$$-\chi\hat{F}_{0\theta\theta\theta\theta}+6v^2\chi\hat{F}_{0\theta\theta}, \tag{80}$$

$$\mathrm{Im}K(\hat{F}_0) = -\hat{F}_{0T}-4v\chi\hat{F}_{0\theta\theta\theta}+4v^3\chi\hat{F}_{0\theta}). \tag{81}$$

As $\hat{F}_{0\theta}$ and $\hat{F}_0$ are solutions of the homogeneous part of Eqs. (78) and (79), respectively, we have the secularity conditions

$$\int_{-\infty}^{\infty}\hat{F}_{0\theta}\,\mathrm{Re}K(\hat{F}_0)\,\mathrm{d}\theta=0, \tag{82}$$

$$\int_{-\infty}^{\infty}\hat{F}_0\,\mathrm{Im}K(\hat{F}_0)\,\mathrm{d}\theta=0. \tag{83}$$

By substituting the values of $\hat{F}_0$, $\hat{F}_{0\theta}$, $\mathrm{Re}K(\hat{F}_0)$, and $\mathrm{Im}K(\hat{F}_0)$ into Eqs. (82) and (83), and after evaluating the integrals, we obtain $A_T=v_T=0$, which imply that developing the Taylor series expansion to the fourth order (this means giving more precision to our results) has no effect on the velocity and amplitude of the soliton in our system during propagation.

The perturbed soliton solution can now be constructed by solving Eqs. (78) and (79). The homogeneous part of Eq. (78) admits the following two particular solutions

$$\phi_{11} = \mathrm{sech}A(\theta-\theta_0)\tanh A(\theta-\theta_0), \tag{84}$$

$$\begin{aligned}\phi_{12} = {}&(-1/A)[\mathrm{sech}A(\theta-\theta_0)\\ &-(3A/2)(\theta-\theta_0)\,\mathrm{sech}A(\theta-\theta_0)\tanh A(\theta-\theta_0)\\ &-(1/2)\sinh A(\theta-\theta_0)\tanh A(\theta-\theta_0)].\end{aligned} \tag{85}$$

Using the above two particular solutions, the general solution of Eq. (78) can be found using the formula

$$\begin{aligned}\phi_1 = {}&k_1\phi_{11}+k_2\phi_{12}-\phi_{11}\int_{-\infty}^{\theta}\phi_{12}\,\mathrm{Re}K(\hat{F}_0)\,\mathrm{d}\theta\\ &+\phi_{12}\int_{-\infty}^{\theta}\phi_{11}\,\mathrm{Re}K(\hat{F}_0)\,\mathrm{d}\theta,\end{aligned} \tag{86}$$

where k_1 and k_2 are arbitrary constants. By substituting the values of ϕ_{11}, ϕ_{12}, and $\mathrm{Re}K$ into Eq. (86) and by evaluating the integrals, we obtain ϕ_1 as

$$\begin{aligned}\phi_1 = {}&(1/16A)\,\mathrm{sech}^5A(\theta-\theta_0)\{11A^4\chi-3(v\theta_{0T}+\sigma_{0T}+\chi v^4)\\ &+4(A^4\chi-v\theta_{0T}-\sigma_{0T}-\chi v^4)\cosh 2A(\theta-\theta_0)\\ &+A(A^4\chi-6A^2v^2\chi+v\theta_{0T}+\sigma_{0T}+\chi v^4)(\theta-\theta_0)\\ &\times[2\sinh 2A(\theta-\theta_0)+\sinh 4A(\theta-\theta_0)]\\ &+16k_1A\cosh^3A(\theta-\theta_0)\sinh A(\theta-\theta_0)\\ &+2k_2[12A(\theta-\theta_0)\sinh A(\theta-\theta_0)-9\cosh A(\theta-\theta_0)\\ &-(\chi v^4+7A^4\chi+v\theta_{0T}+\sigma_{0T})\cosh 4A(\theta-\theta_0)\\ &+\cosh 3A(\theta-\theta_0)]\cosh^3A(\theta-\theta_0)\}.\end{aligned} \tag{87}$$

The term proportional to k_2 in that solution is a secular term that makes the solution unbounded and, hence, it is removed by choosing the arbitrary constant k_2 =0. Using the boundary conditions

$$\phi_1\,|_{\theta=\theta_0=0}=\phi_{1\theta}\,|_{\theta=\theta_0=0}=0,$$

we obtain $k_1=0$ and $(v\theta_{0T}+\sigma_{0T})=\chi(A^4-v^4)$. Taking into account these analyses, the real part of the perturbed soliton is found to be

$$\begin{aligned}\phi_1 = {}&\chi A^2[(A^2-3v^2)(\theta-\theta_0)\cosh A(\theta-\theta_0)\\ &-4A\sinh A(\theta-\theta_0)]\\ &\times\mathrm{sech}^2A(\theta-\theta_0)\tanh A(\theta-\theta_0).\end{aligned} \tag{88}$$

In a similar way, the homogeneous part of Eq. (79) admits the following two particular solutions

$$\psi_{11} = \mathrm{sech}A(\theta-\theta_0), \tag{89}$$

$$\begin{aligned}\psi_{12} = {}&(1/2A)[\sinh A(\theta-\theta_0)\\ &+A(\theta-\theta_0)\,\mathrm{sech}A(\theta-\theta_0)].\end{aligned} \tag{90}$$

Equation (79) can then be solved by constructing the general solution in the form

$$\begin{aligned}\psi_1 = {}&\kappa_3\psi_{11}+\kappa_4\psi_{12}-\psi_{11}\int_{-\infty}^{\theta}\psi_{12}\,\mathrm{Im}K(\hat{F}_0)\,\mathrm{d}\theta\\ &+\psi_{12}\int_{-\infty}^{\theta}\psi_{11}\,\mathrm{Im}K(\hat{F}_0)\,\mathrm{d}\theta,\end{aligned} \tag{91}$$

where κ_3 and κ_4 are arbitrary constants. Following the same procedure, we integrate the integrals and remove the secular term by choosing the arbitrary constant $\kappa_4=0$ and apply the following boundary conditions

$$\psi_1\,|_{\theta=\theta_0=0}=\psi_{1\theta}\,|_{\theta=\theta_0=0}=0.$$

We obtain $\kappa_3=0$ and $\theta_{0T}=-4v\chi(2A^2+v^2)$. Using these results, the final form of the general solution ψ_1 is obtained as

$$\begin{aligned}\psi_1 = {}&6\chi A^2v[\sinh A(\theta-\theta_0)-A(\theta-\theta_0)\\ &\times\cosh A(\theta-\theta_0)]\,\mathrm{sech}^2A(\theta-\theta_0).\end{aligned} \tag{92}$$

From Eqs. (88) and (92), the first-order perturbed part of the soliton $\hat{F}_1=\phi_1+\mathrm{i}\psi_1$ is obtained as

$$\begin{aligned}\hat{F}_1 = {}&\chi A^2\{[(A^2-3v^2)(\theta-\theta_0)\cosh A(\theta-\theta_0)\\ &-4A\sinh A(\theta-\theta_0)]\tanh A(\theta-\theta_0)\\ &+\mathrm{i}6v[\sinh A(\theta-\theta_0)-A(\theta-\theta_0)\\ &\times\cosh A(\theta-\theta_0)]\}\,\mathrm{sech}^2A(\theta-\theta_0).\end{aligned} \tag{93}$$

Knowing $\hat{F}_1$, we can write the general first-order perturbed soliton solution

$$F=(\hat{F}_0+\varepsilon\hat{F}_1)\,\mathrm{e}^{\mathrm{i}[v(\theta-\theta_0)+(\sigma-\sigma_0)]}$$

of Eq. (74), and deduce for $\varepsilon=1$ and $r>5$ the general expression of a wave in our system

$$f(z,t)=(B_1/B_2)^{1/2}F(z,t)\,\mathrm{e}^{-\mathrm{i}(2\beta+4g)t}. \tag{94}$$

In Fig. 7(a), we have plotted the square of the absolute value of f and we find that the nature of the soliton is not very perturbed by the increasing of the order of Taylor expansion, even if its expression shows that its amplitude has changed (see Eq. (94). As we can note in Fig. 7(b), the behavior of $|f|^2$ as a function of LRI's parameter remains unchanged.

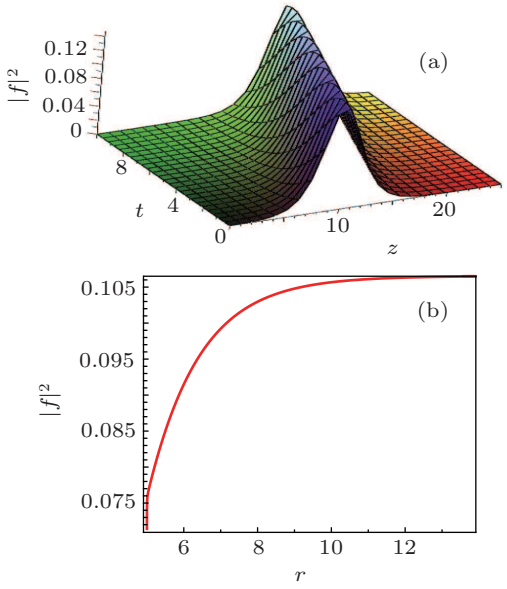


Fig. 7. (color online) (a) Breather-like solitonic wave for the fourth order Taylor expansion. (b) Evolution of the bubble amplitude as a function of LRI's parameter for the fourth order Taylor expansion.

Due to the complexity of Eqs. (70)–(73), the appropriate resolution methods are not yet found. We are still trying to solve them. But in the meantime, to satisfy these conditions, we solve the set of discrete Eqs. (34)–(36) using the numerical simulations, which take into account all the ranges of interaction between bases.

6. Numerical results

Numerical simulations allow getting round the problem of the order of derivative by solving directly the set of discrete equations

$$\begin{aligned} \mathrm{i}\hbar\dot{f}_n &= -\sum_{m\neq n}\Omega_{m,n}(f_m - f_n) + g(f_{n+h} + f_{n-h} + 2f_n) \\ &\quad -[2\alpha_1(x_{n+1} - x_{n-1}) \\ &\quad +\alpha_2(y_{n+1} - y_{n-1}) - 2\beta]f_n, \qquad (95) \\ m_{\mathrm{H}}\ddot{x}_n &= 2K_{\mathrm{H}}(x_{n+1} + x_{n-1} - 2x_n) \\ &\quad +4\alpha_1(|f_{n-1}|^2 - |f_{n+1}|^2), \qquad (96) \\ m_{\mathrm{p}}\ddot{y}_n &= 2K_{\mathrm{p}}(y_{n+1} + y_{n-1} - 2y_n) \\ &\quad +2\alpha_2(|f_{n-1}|^2 - |f_{n+1}|^2). \qquad (97) \end{aligned}$$

Before comparing numerical and theoretical results, we first discuss briefly the numerical technique. The idea of this section is based on the fact that many works and experiences have already shown that breather-like solitons govern the DNA's transcription process, as we have obtained in the previous sections of this work. Then, we basically perform the simulation by using a continuum breather as an initial condition in the discrete DNA lattice with HC and LRI. It can be seen as the simulation of the ensuing propagation of the pulse, solving the perturbed NLS equation with a fourth-order Runge–Kutta method, where

$$f_n(0) = \begin{cases} F_0\ \mathrm{sech}[(1/L_{\mathrm{e}})n + A_0]\exp \mathrm{i}\,\theta_0, & \text{for } n_1 \leq n \leq n_2, \\ 0, & \text{otherwise}, \end{cases} \qquad (98)$$

$$x_n(0) = f_n(0), \quad \text{for all } n, \qquad (99)$$

$$y_n(0) = f_n(0), \quad \text{for all } n, \qquad (100)$$

$$\dot{x}_n(0) = \dot{y}_n(0) = 0, \quad \text{for all } n. \qquad (101)$$

The parameters F_0, L_{e}, θ_0, and A_0 remain the same as in Section 3, and as mentioned in Section 2, the numerical values of the model parameters are those used in Refs. [38], [44]–[51]. The numerical values of n_1 and n_2 are inspired from the results of Section 3 and are considered to be $n_1 = 20$ and $n_2 = 31$; this means that the initial breather is formed by 12 base pairs. The periodic boundary conditions are used by considering a system involving fifty base pairs. The time step has been chosen as $\Delta t = 10^{-5}$, which implies that the total accumulated error is approximately 10^{-20} in our results.

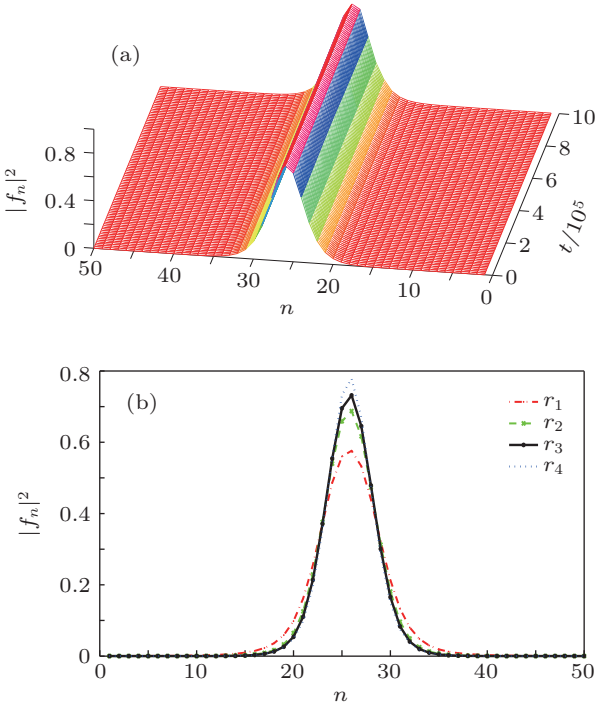


Fig. 8. (color online) Results for numerical simulations: (a) 3D-evolution of the square of the amplitude in the space and in the time. (b) Evolution of the bubble feature as a function of LRI's parameter. $r_1 = 2.01$, $r_2 = 3.7$, $r_3 = 5$, and $r_4 = 17$.

We have plotted the 3D evolution of our specimen in Fig. 8(a). The figure shows that numerical simulations confirm the presence of breather-like solitons during the transcription process. The results obtained in the previous sections can also be confirmed by observing Fig. 8(b), which represents the evolution of the square of the amplitude of the bubble-soliton in our specimen during the increasing of LRI's parameter r. Indeed, the width of the bubble decreases while its height increases when the LRI's parameter increases. We have also noted, as obtained previously, that strong HC coupling leads

to a highly localized longitudinal wave with high amplitude while weak HC leads to a small amplitude localized longitudinal wave with large spatial expansion.

7. Conclusion

In summary, we have investigated in this paper the effects of HC and power-law LRI between intra-strand nucleotides in the nonlinear dynamics of the DNA double helix. We have considered a situation in which RNAP approaches the DNA molecule at physiological temperature and creates the bubble. The B-form of the DNA molecule is assimilated to the Heisenberg model for a coupled anisotropic site-dependent spin system and an RNAP is treated as a single linear molecular chain interacting with DNA through linear coupling. A single molecule of RNAP is then allowed to move linearly along the DNA molecule. The dynamics is then derived in the form of coupled nonlinear evolution equations after bosonizing the Hamiltonian using Holstein–Primakoff representation of spin operators, which finally reduces to the completely integrable NLS equation that admits soliton solutions. We have concluded from the condition for obtaining breather-like solution that the HC is weak compared to intra-strand coupling in the real DNA molecule. The importance of the helical structure and LRI are brought out by analyzing realistic effects of both couplings on that breather-like solution, and results show that they lead to a drastic change of the soliton properties. The key finding in this analysis is that by increasing the HC force or the LRI parameter, the bubble height will be enhanced while its width is reduced. These results are confirmed by numerical simulations and are in agreement with the experimental data obtained in Refs. [63]–[66]. We have also found that the number of base pairs which participate in the opening of the DNA's strands has a strong overlap with experimental studies. The localized solitons we have studied in the present work are usually used to explain the open-states in DNA molecule when an RNAP acts with it at the biological temperature, within the process of transcription. Several authors suggested that the breathers modes have a realistic meaning in DNA nonlinear modes.[71,72] In our opinion, taking into account HC and LRI in the DNA molecule as in the present work, can be considered as a much better representation of RNAP-DNA dynamics than those which do not consider these interactions.

Fluctuating thermal openings of the double helix of DNA (bubbles) are known to exist in a regime extending well below the denaturation, which includes physiological temperatures. These openings could be exploited by regulatory proteins or functional enzymes to perform their work.[73] However, recently it was argued that thermodynamic characterization of the thermal fluctuations may differ from a dynamical characterization, which points to the need for a thorough understanding of the dynamical effects in this highly nonlinear and cooperative material. It has been suggested that there is an increased probability for large bubbles to appear at functionally relevant sites of gene promoter DNA segments.[74] The distribution of bubble lengths ranging from 0.34 nm (single base-pair openings) up to a few tens of nanometers (corresponding to openings of size of several tens of base pairs) has been presented.[75] The bubble length distributions have been obtained with Monte Carlo simulations and with the Langevin dynamics, using the Peyrard–Bishop–Dauxois model for describing the energy of base-pair openings.[75] The bubble length distribution depends on the Guanine–Cytosine content. It is the fraction of GC base pairs in the sequence. The variation of the distribution as a function of the GC content will be investigated in a two-coupled spin chain model or spin ladder system for DNA. In that work, we will study how the exponent which characterizes the bubble sizes is influenced by the LRI and the HC. The results will be discussed in the framework of the Poland–Scheraga and the Peyrard–Bishop–Dauxois models. In addition, the two different base pairs of the real DNA, A–T, and G–C, combine in different ways constituting the genetic code. In nature, the presence of different sites along the strands (such as coding, promoter and terminator sites which have the very specific sequences of bases and particular functions) makes the strands site-dependent or inhomogeneous. It is also necessary to study the modulational instability from a statistical point of view.[76] Then, in the more realistic study, it is important to include these influences in the RNAP-DNA dynamics. In these fields, studies are under progress.

References

[1] Davydov A 1981 *Solitons in Molecular Systems* (Dordrecht: Kluwer)
[2] Englander S, Kallenbach N, Heeger A, Krumhansl J and Litwin A 1980 *Proc. Natl. Acad. Sci. USA* **77** 7222
[3] Kalosakas G, Rasmussen K Ø and Bishop A R 2004 *Synth. Met.* **141** 93
[4] Yakushevich L V 1994 *Physica D* **79** 77
[5] Yakushevich L V 2004 *Nonlinear Physics of DNA* (Berlin: Wiley-VCH)
[6] Stryer L 1995 *Biochemistry*, 4-th edn. (New York: W. H. Freeman and Company)
[7] Dauxios T 1991 *Phys. Lett. A* **159** 390
[8] Xia J F and Jia Y 2010 *Chin. Phys. B* **19** 040506
[9] Tabi C B, Mohamadou A and Kofané T C 2009 *Chin. Phys. Lett.* **26** 68703
[10] Zayed E M E and Arnous A H 2012 *Chin. Phys. Lett.* **29** 080203
[11] Cadoni M, Leo R De and Gaeta G 2007 *Phys. Rev. E* **75** 021919
[12] Baverstock K F and Cundall R B 1988 *Nature* **332** 312
[13] Salerno M 1991 *Phys. Rev. A* **44** 5292
[14] Qian J, Xie P, Xue X G and Wang P Y 2009 *Chin. Phys. B* **18** 4852
[15] Yan X L and Dong R X 2007 *Chin. Phys.* **16** 2062
[16] Gao J and Xue Z Y 2009 *Chin. Phys. B* **18** 370
[17] Peyrard M, Lopez S C and James G 2009 *J. Biol. Phys.* **35** 73
[18] M Salerno 1992 *Phys. Lett. A* **167** 49
[19] Han J J and Fu W J 2010 *Chin. Phys. B* **19** 010205
[20] Zhou Q and Chen Z Q 2010 *Chin. Phys. B* **19** 090508
[21] Gueron M, Kochoyan M and Leroy J J 1987 *Nature* **328** 89
[22] Daniel M and Vasumathi V 2007 *Physica D* **231** 10
[23] Fujimoto S and Yu Y X 2010 *Chin. Phys. B* **19** 088701
[24] Yan Y Y and Zhu P 2011 *Chin. Phys. B* **20** 018701

[25] Vasumathi V and Daniel M 2009 *Phys. Rev. E* **80** 061904
[26] Dandoloff R and Saxena A 1997 *J. Phys.*: *Condens. Matter* **9** L667
[27] Homma S and Takeno S 1983 *Prog. Theor. Phys.* **70** 308
[28] Takeno S and Homma S 1984 *Prog. Theor. Phys.* **72** 679
[29] Zdravkovic S and Sataric M V 2001 *Phys. Scr.* **64** 612
[30] Zdravkovic S and Sataric M V 2003 *Int. J. Mod. Phys. B* **17** 5911
[31] Tabi C B, Mohamadou A and Kofane T C 2008 *J. Phys.: Condens. Matter* **20** 415104
[32] Zdravkovic S and Sataric M V 2007 *Europhys. Lett.* **78** 38004
[33] Tabi C B, Fouda H P E and Kofane T C 2011 *J. Comput. Theor. Nanosci.* **8** 1
[34] Woafo P, Kofané T C and Bokosah A S 1992 *J. Phys.: Condens. Matter* **4** 3389
[35] Tchawoua C, Kofané T C and Bokosah A S 1993 *J. Phys. A: Math. Gen.* **26** 6477
[36] Saha M and Kofané T C 2012 *Chaos* **22** 013116
[37] Rau D C and Parsegian V A 1992 *Biophys. J.* **61** 246
[38] Larsen P V, Christiansen P L, Bang O, Archilla J F R and Gaididei Yu B 2004 *Phys. Rev. E* **70** 036609
[39] Mingaleev S F, Gaididei Y B and Mertens F G 1998 *Phys. Rev. E* **58** 3833
[40] Daniel M and Beula J 2008 *Phys. Rev. B* **77** 144416
[41] Zdravković S, Tuszyński J A and Satarić M V 2005 *J. Comput. Theor. Nanosci.* **2** 263
[42] Zdravković S 2005 *Finely Dispersed Particles: Micro-, Nano-, and Atto Engineering*, 130 *Surfactant Science Series*, eds. Spasic A M and Hsu J P (Dekker/CRC Press/Taylor & Francis Group) p. 779
[43] Satarić M V, Matsson L and Tuszyński J A 2006 *Phys. Rev. E* **74** 051902
[44] Saha M and Kofané T C 2012 *Int. J. Mod. Phys. B* **26** 1250101
[45] Peyrard M and Bishop A R 1989 *Phys. Rev. Lett.* **62** 2755
[46] Dauxois T, Peyrard M and Bishop A R 1993 *Phys. Rev. E* **47** 684
[47] Fujita H, Imamura A and Nagata C 1974 *J. Theor. Biol.* **45** 411
[48] Zdravkovic S and Sataric M V 2006 *Phys. Rev. E* **73** 021905
[49] Zdravkovic S and Sataric M V 2008 *Phys. Rev. E* **77** 031906
[50] Lawrence A F, Daniel J C Mc, Chang D B and Birge R R 1987 *Biophys. J.* **51** 785
[51] http://www.peptideguide.com/peptide-bond.html
[52] Daniel M and Kavitha L 2002 *Phys. Lett. A* **295** 121
[53] Holstein T and Primakoff H 1940 *Phys. Rev.* **58** 1098
[54] Nguenang J P and Kofané T C 1997 *Phys. Scr.* **55** 367
[55] Nguenang J P and Kofané T C 2000 *Physica D* **147** 311
[56] Glauber R J 1963 *Phys. Rev.* **131** 2766
[57] Rasmussen K Ø, Christiansen P L, Johansson M, Gaididei Yu B and Mingaleev S F 1998 *Physica D* **113** 134
[58] Peyrard M and Bishop A R 1989 *Phys. Rev. Lett.* **62** 2755
[59] Scott A C, Chu F Y F and McLaughlin D W 1973 *Proc. IEEE* **61** 1443
[60] Hasegawa A 1975 *Plasma Instabilities and Nonlinear Effects* (Berlin: Springer)
[61] Zdravkovic S and Sataric M V 2008 *Phys. Lett. A* **373** 126
[62] Takeno S 2005 *Phys. Lett. A* **339** 352
[63] Wang J C, Jacobsen J H and Saucier J M 1977 *Nucleic Acids Res.* **4** 1225
[64] Hsieh T S and Wang J C 1978 *Nucleic Acids Res.* **5** 3337
[65] Melnikova A, Beabealashvilli R and Mirzabekov A D 1978 *Eur. J. Biochem.* **84** 301
[66] Siebenlist U 1979 *Nature* **279** 651
[67] Brunhuber C, Mertens F G and Gaididei Y 2007 *Eur. Phys. J. B* **57** 57
[68] Ishimori Y 1982 *Prog. Theor. Phys.* **68** 402
[69] Kodama Y and Ablowitz M J 1981 *Stud. Appl. Math.* **64** 225
[70] Beula J and Daniel M 2010 *Physica D* **239** 397
[71] Jurnak F A and McPherson A 1985 *Structure of Biological Macromolecule and Assemblies* (New York: John Wiley and Sons Inc.) **2** p. 172
[72] Krusmhansl J A, Wysin G M, Alexander D M, Garcia A, Lomdahl P S and Layne S P 1985 *Structure and Motion: Menbrane, Nucleic Acids and Proteins*, eds. Sarma M H and Sarma R H (New York: Academic Press) p. 407
[73] Banerjee A and Sobell H M 1983 *J. Biomol. Struct. Dyn.* **1** 253
[74] Choi C H, Kalosakas G, Rasmussen K ϕ, Hiromura M, Bishop A R and Usheva A 2004 *Nucleic Acids Res.* **32** 1584
[75] Ares S and Kalosakas G 2007 *Nano. Lett.* **7** 2
[76] Visinescu A and Grecu D 2004 *Proc. Inst. Math. NAS Ukraine* **50**, Part 3, p. 1502